URTeC: 2154977

Predicting Frac Performance and Active Producing Volumes Using Microseismic Data

Charles Sicking, Jan Vermilye, Alfred Lacazette, Global Geophysical Services, Inc.

Summary

We present an approach for managing unconventional reservoirs that uses passive seismic recordings captured on time intervals of months similar to 4D surface reflection surveys. Computing the producing volume at regular intervals over the years of production allows for better decisions on the design of the frac treatments for future wells and for the determination of where to do infill drilling. The installation of a shallow buried grid over the reservoir provides for efficient recording of the data at the times required for monitoring frac treatments and for computing the producing volumes. Using fracture imaging, the fracture systems in the reservoir are computed before the frac treatment, during frac treatment, and during production. A byproduct of the fracture imaging method is the ability to store the first time of activation for each segment of each fracture. This allows for detailed analysis of how the rocks are fracturing. In addition to monitoring unconventional reservoirs the method is being used for monitoring CO2 injection. It has been used for reservoir fluid flow monitoring and can be used for monitoring cuttings disposal wells to track the movement of fluids.

Introduction

The fracture imaging method is a new product that was introduced to passive data processing about 10 years ago. It has been used to map fractures and fluid flow under for many applications. Maps of the natural fractures in the rocks are made on a large area scale to determine the location of fracture permeability zones before drilling. Using fracture imaging to track the induced fractures that are activated during frac treatments is a very important product that has become popular in the development of unconventional reservoirs. The method is used for monitoring the fluid flow during water flooding and for mapping the flow of CO2 in the subsurface for CO2 sequestration. Other applications that are being pursued include monitoring of the subsurface around cuttings injection wells, monitoring for collapse features, and detecting water flow into mines.

Previous publications describe the fracture imaging method. See for example: Geiser, et.al., 2012; Lacazette, et.al., 2013; Sicking, et.al., 2012; and Sicking, et.al, 2014. The method uses streaming depth imaging to compute depth volumes for each of the defined time windows of the recorded trace data that cover the clock time interval of interest. For each time window, an image is computed for all of the voxels in the depth volume. The many depth volumes are edited and then combined to make a single depth volume that is used to compute the fracture image volume. Steps for computing the fracture image volumes include data acquisition, velocity model building, trace processing for noise suppression, imaging, and fracture image computation. These steps are briefly reviewed in the following sections. This paper focuses on the value of using passive recordings for: the prediction of frac treatment performance before the actual treatment; the focusing of the seismic emissions during the frac treatment for estimating the volume of rock that is stimulated; mapping the time sequential activation of the fractures during treatment; and on the measurement of the active producing volume over time of production. Mapping the producing volume over time is analogous to 4D surface seismic in that it measures the changes in the producing reservoir.

Passive data acquisition

The passive data used in the fracture imaging method can be recorded with a surface grid or with a buried grid of geophones. The method is very sensitive to surface waves that are noise in this case. The design of the grid for recording the passive data is an important component for detection and accurate location of both Micro-EarthQuakes (MEQ) and fracture networks. Generally, the optimum grid design is a uniform distribution of geophones covering the required aperture. Experience shows that for good quality imaging, a radial aperture of 1.5 to 2.0 times the target depth should be used. The detectability of the passive seismic emissions depends on the S/N ratio of the trace data after filtering has been applied to suppress the various types of noise. For good detection, the signal level of the seismic energy arriving from the subsurface must have amplitudes similar to the noise in the traces after the coherent noise and other noise have been removed. One of the best methods for suppressing surface wave noise is to use a uniform grid for acquisition. This is illustrated in Figure 1 which shows two images of a depth slice computed for the same field data but recorded simultaneously using a star grid and an orthogonal grid. A highway cuts through the grid and is the source of significant surface wave noise. The image computed using the star grid shows a large footprint of the highway noise because the noise is hitting the grid perpendicular to the arms. The depth slice computed using the orthogonal grid does not show this high level of coherent noise from the highway and the seismic emissions that are generated by the frac treatment at the stage location are much better focused

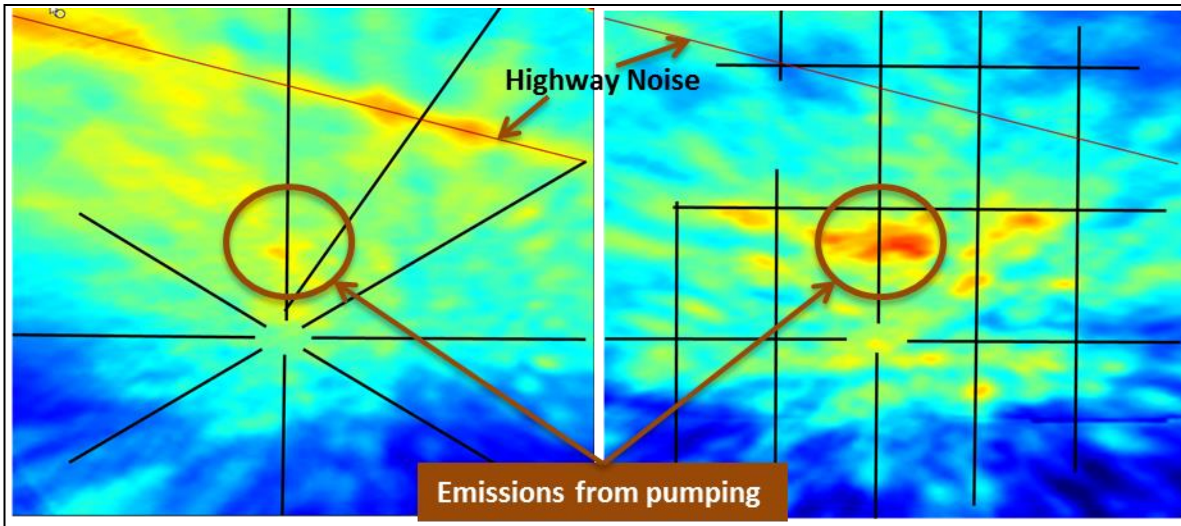

Figure 1: Comparison of highway noise footprint in the image volume for recording with a star grid and with an orthogonal grid. The noise hits the star grid perpendicular to the linear arrays of the grid arms and passes the coherent nose into the image. The orthogonal grid samples the noise at multiple azimuths and the surface wave noise from the highway is suppressed and not passed into the image.

Velocity model and statics

The velocity model must be accurate in order to obtain correct locations for the fractures in the volume. Often, a 1D P-wave velocity model is constructed from a nearby sonic log and the focusing is performed using a 1D velocity model. This works very well for the small area around the well, especially if the strata are horizontal and relatively homogeneous. When there is a lateral velocity gradient, the location accuracy can be degraded. However, if the magnitude of the velocity gradient is estimated from perf shot location accuracy, beam steering methods can be used in the imaging to compute accurate locations. Figure 2 shows a vertical cross section of two velocity models. The top image shows a smooth lateral velocity gradient in the Eagle Ford and the bottom image shows a complex 3D velocity model from a thrust-related fault bend-fold anticline. When the velocity model has 3D complexity, the full-volume 3D interval velocity must be used for all aspects of focusing and imaging in order to obtain useful results.

The total statics for passive recording consist of two parts. First, the correction for the receiver elevation is computed from the known elevation of the receivers and the near surface velocity. Quality control of the elevation correction comes from observing the waveform alignment of perf shots with known locations. Second, there are always residual time errors in the flattened perf waveforms or MEQ and these residuals must be corrected in order to obtain the best results from the fracture imaging workflow. Figure 3 shows the waveforms for a perf shot before and after residual statics have been applied.

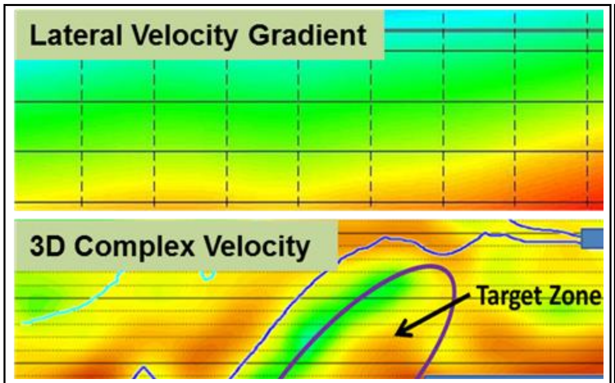

Figure 2: Velocity models for fracture imaging. The top panel shows a model that has a lateral velocity gradient. The bottom panel shows a complex 3D velocity model.

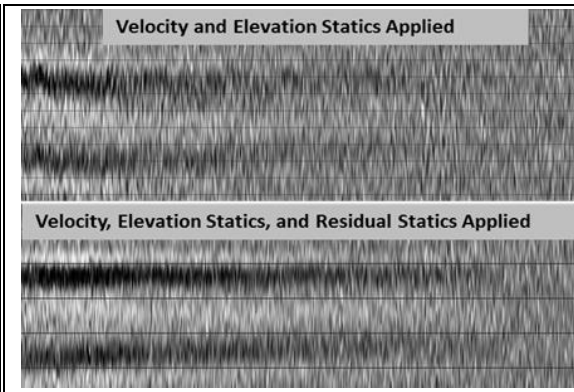

Figure 3: Waveforms for a perf shot recorded on a surface grid. Top panel does not have residual statics applied. Bottom panel is the same data with residual statics.

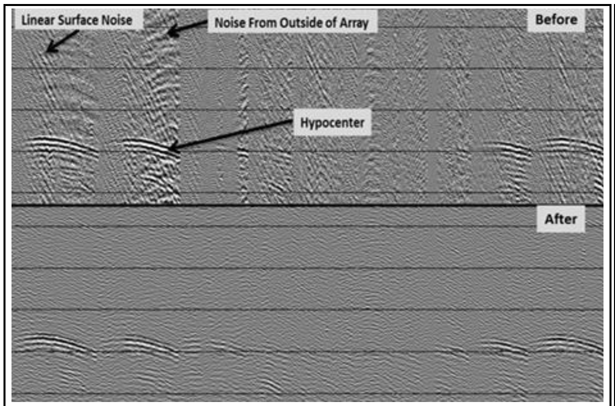

Figure 4: Top panel shows the raw trace data with surface waves from the well head and surface waves from outside of the grid. Bottom panel is the same trace data with the noise removed.

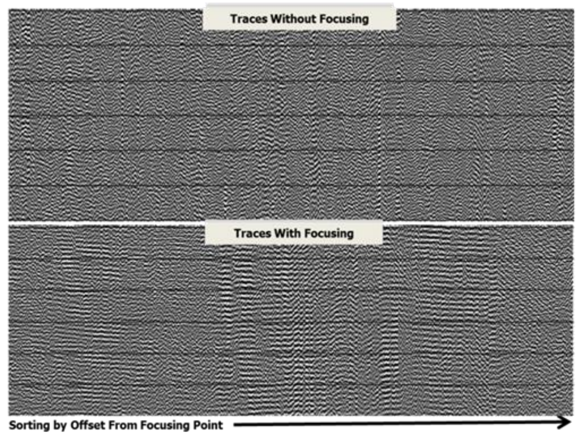

Figure 5: Long Duration Signals (LDS) contribute most of the signal to the fracture images.

Trace processing and noise removal

Removing the coherent surface wave noise is critically important for good imaging results from a surface recording. The detectability of the radiated seismic energy depends on the S/N ratio of the trace data after filtering has been applied to suppress the various types of noise. Figure 4 shows the raw trace data in the top panel and the filtered trace data in the bottom panel for the cables of a star array design. The raw trace data shows the surface wave noise propagating out from the well head as a linear move out from near to far on the cables. There is additional coherent surface wave noise propagating from outside of the array. This latter noise is not moving in line with the cables and shows move out from far offset to near offset on the second cable. This same noise on the first cable shows that the surface waves are propagating perpendicular to the cable. For good focusing, the surface wave noise must be removed. The bottom panel of Figure 4 shows the trace data after the removal of both the surface noise from the well head and the surface noise from outside the grid.

Long duration signals (LDS)

LDS are continuous seismic waveforms originating in the reservoir and lasting for seconds or minutes and are episodic and pulsating in nature. These waveforms are similar to those documented by Das and Zobach, 2013. However, these LDS waveforms are not precursors to MEQ occurrences. MEQ signals are by definition of short duration and have higher amplitudes than LDS waveforms. During pumping, there is a large fluid flow and a large pressure change at the frac stage location. This fluid flow and differential stress causes seismic signals from the frac stage location in the form of LDS waveforms. This signal has been studied in detail for two stages of a frac treatment project. For each of the two stages, LDS were tracked and demonstrated to exist for 60% of the minutes in the 100 minutes of pump time. The LDS are very episodic and sporadic. Tary et.al, 2012 and Tary et.al. 2014 document similar signals recorded in frac data. They appear and disappear on time scales ranging from seconds to many minutes in duration. An example of a LDS is shown in Figure 5. Only a few seconds of trace data are shown in Figure 5. The frequency range of positive S/N for LDS is from 15 to 55 Hz. This frequency band is the same as the dominant frequency band observed for surface reflection data.

Fracture imaging workflow

The fracture imaging method can be best described as a one-way travel time Pre-stack Depth Migration (PSDM). The signals travel one-way from the reservoir to the receiver. For surface reflection seismic data the signal travels over a two-way path from the source to the reservoir and back to the receiver. Passive seismic and reflection seismic require the same velocity and statics models. However, there are significant differences. Passive seismic involves

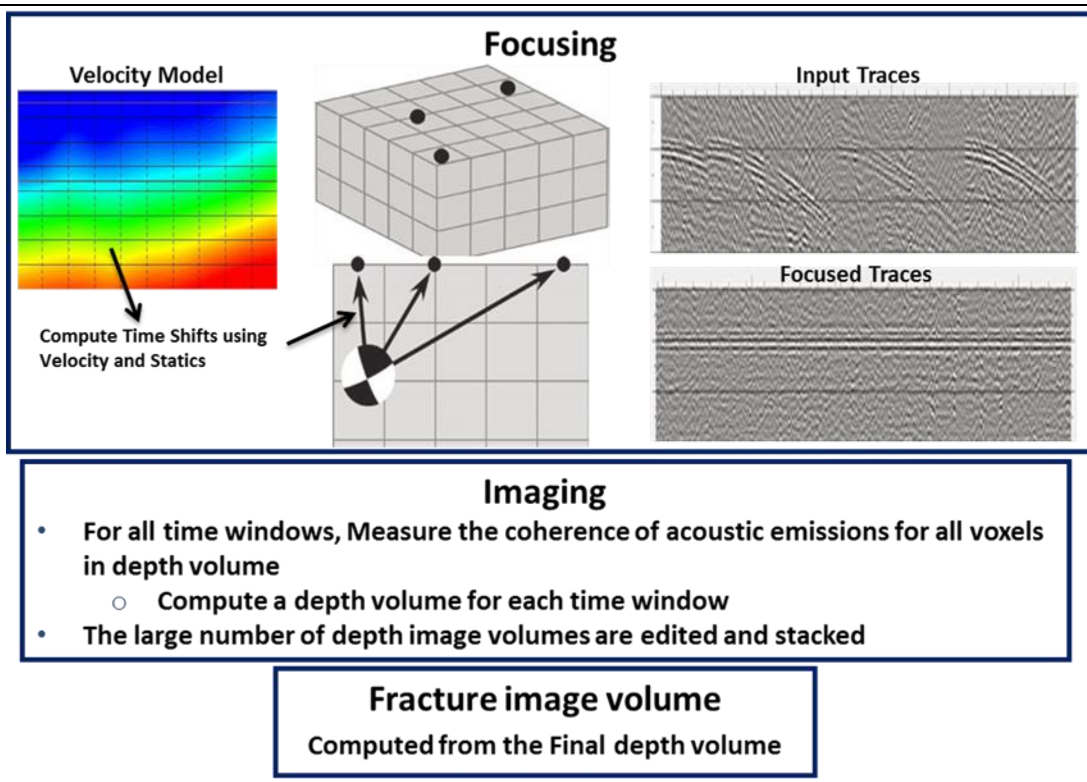

Figure 6: The fracture imaging workflow has 5 parts. The first part computes the travel times from each depth voxel to each receiver in the recording grid. The second part shifts the traces in time by the computed travel times. The third part computes the image value. The fourth part combines all of the depth volumes into one volume. The fifth part computes the fracture image volume. The total clock time of the passive recording is broken into many time windows. Each time window is focused and a single depth volume is computed for that time window. The number of depth volumes computed is equal to the number of time windows.

one-way travel time through the Earth and the signals of interest are direct arrivals unrelated to the reflections at impedance boundaries. In addition, passive signals suffer attenuation only from one transmission though the Earth.

The attenuation of reflection seismic signals is double that of passive data and the energy reflected from the impedance boundaries is small compared to the direct energy from the source. For passive seismic signal, the key spatial parameters, *x, y, z*, and the *time* parameter are all unknown. In order to image the passive signals, the time of investigation and the spatial volume for investigation must be chosen. The depth volume for the entire time window of interest is imaged by streaming the passive signal through the depth imaging algorithm that sequentially focuses every smaller time window of the total time of investigation into every depth voxel being investigated. The streaming method focuses all of the seismic signals that come from each voxel into multiple depth volumes and the signals for each voxel of the volume are integrated over all of the time windows. The result is a single depth volume that is used to extract the volumetric fracture images for the depth volume. This single final depth volume contains the fracture surfaces that are extracted to compute the volumetric fracture images.

The workflow for fracture imaging is shown in Figure 6. The steps are computation of the travel times from each depth voxel to each receiver using the velocity model and statics, focusing the trace data by time shifting the traces using the travel times for each voxel, and computing the image value for each voxel. The process is repeated for each time window of investigation whereby the time windows cover the entire time interval of interest. Many depth volumes are computed. These depth volumes are edited and then stacked together to make a single depth volume for input to the fracture image volume computation.

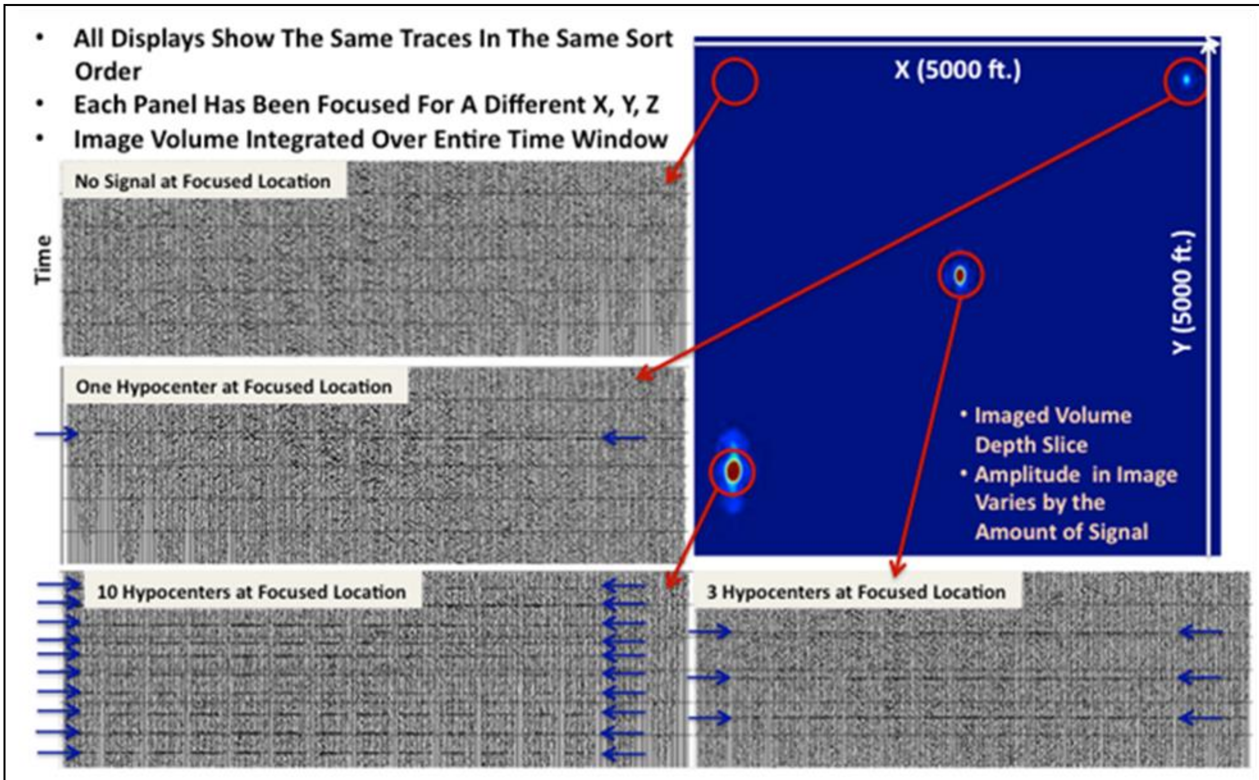

Figure 7: The trace data shown here is from a wave equation synthetic. The four panels of trace data are the same traces and sorted exactly the same for each panel. The traces are focused on four different X, Y locations in the depth volume of investigation. The four locations are shown in the image slice by the four red circles. The arrows point to the traces panel focused for that location. A synthetic signal was imposed in the traces at each location. In the upper left corner of the depth slice there was no signal. In the upper right location there was one impulse in the data. The middle location has three impulses and the lower left location has ten impulses. All impulses occur within the same time window and the integration is across that time window.

The imaging of each voxel for each time window is illustrated using synthetic data in Figure 7. The trace panel was generated using a wave equation modeling program. An impulse was generated at the reservoir depth and the response was recorded at each receiver at the surface of the Earth. The impulse response was modeled at three different X, Y locations at the depth of the reservoir. All three impulses occurred within the same time window of the trace data. The signal for each of the locations is imaged using the depth imaging method and the signal for each location focuses to the voxel in the depth volume for the source of that impulse. Multiple impulses were inserted in the trace panel for each of the three locations. The location with only one impulse is much weaker than the image at the location with ten impulses. The depth volume accurately maps the locations of the impulses and shows that the integration process combines all of the impulses at a single location to build up the signal and suppress the noise.

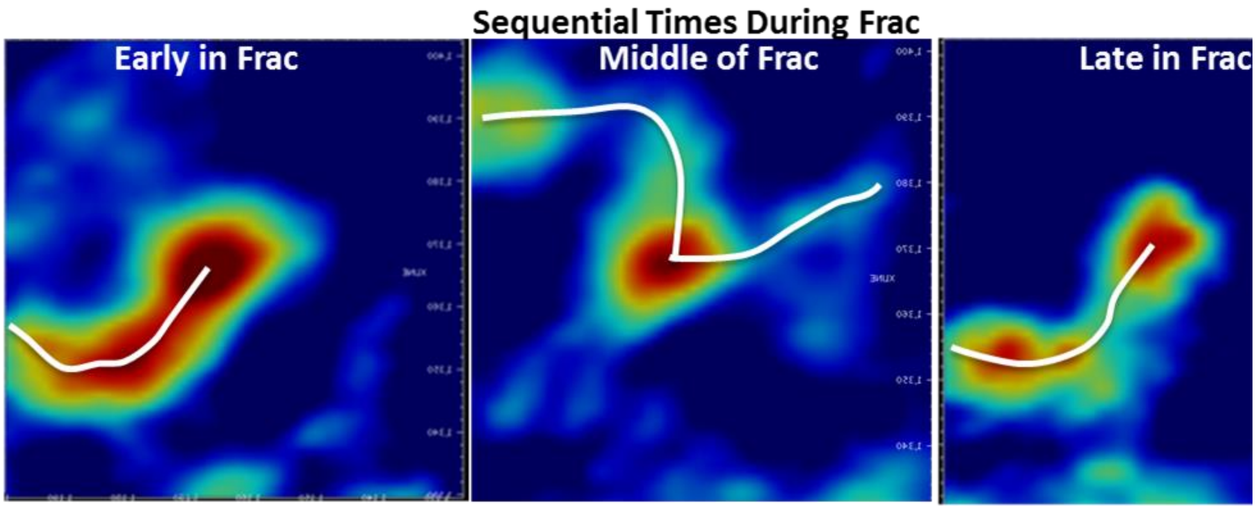

Figure 8: Stage pump time imaging. The same fracture is activated at two separate times during pumping. Each image shows a depth slice at the well depth of the imaged volume and is centered on the stage pump location. Each image is the integration over three minutes of pump time. The left image is data at 30 minutes after start of the stage pumping. The middle image is data at 45 minutes after the start of pumping. The right image is data at 70 minutes after start of stage pumping. Note that the amplitude of the first activation is much larger than the amplitude in the second activation of the fracture.

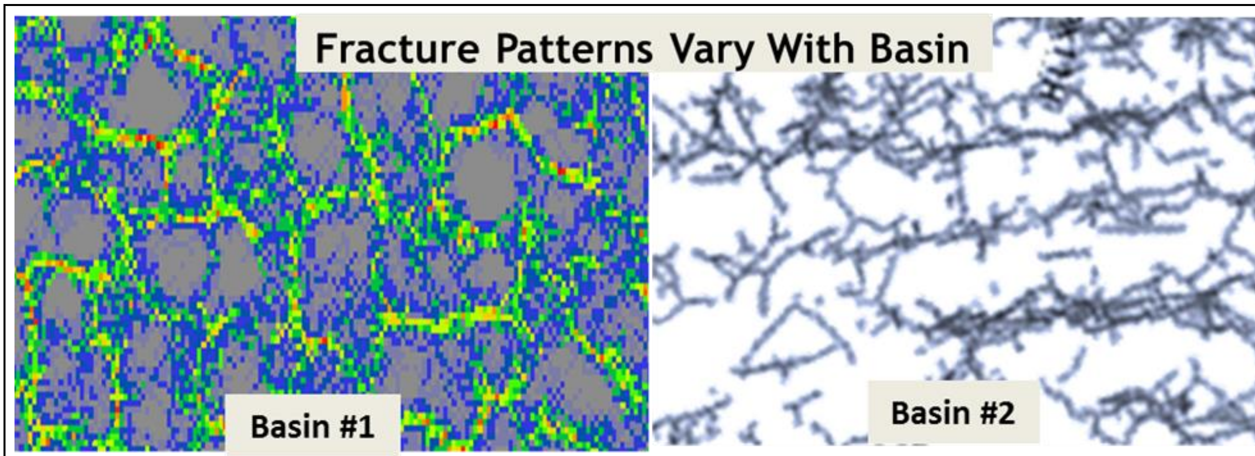

Figure 9: Fracture images are computed for many time intervals. Each time interval is typically hours long. For a frac treatment with 20 stages, a fracture image is computed for each stage so there are 20 fracture images. Merging the 20 fracture images and counting the number of times each voxel is active allows for the evaluation of the location accuracy and resolution of the fracture imaging process. Measuring the density distribution perpendicular to a fracture surface provides the raw data for the analysis. In addition, these images show the fracture patterns for area and making these images for many projects shows the differences in fracture patterns between basins.

Figure 8 illustrates the episodic nature of the fracturing process. The left image shows the integration of signals from the stage pump location for three minutes of pump time at 30 minutes after the start of pumping. The middle image shows the integration of signals from the stage location for three minutes about 45 minutes after the start of the pumping. The right image in Figure 8 shows the integration of signals from the stage pump location for three minutes of pump time at 70 minutes after the start of pumping. These images illustrate that the same fracture activates multiple times during pumping and there is a quiet time when the pressure is rebuilding in that fracture.

Fracture patterns and location accuracy

The fracture imaging method is used to compute an area wide fracture image volume for each stage of a frac treatment. The expectation is that the natural fracture in the rock will be the same for all time intervals of the frac. Computing the areal fracture network for the time interval for each stage allows for the estimation of the location accuracy and resolution of the imaging system. Merging all of the areal fracture images computed and counting the number of times each voxel is activated for all of the fracture images yields the images shown in Figure 9. This figure shows examples of fracture images for two different basins. There are two observations that can be made from this figure. First, different basins have substantially different natural fracture patterns and, second, some fracture patterns are well focused while others are more distributed. Basin 1 in the figure shows the same fractures repeating many times in a tight spatial distribution for the separate estimates. Basin 2 shows that the fractures are spatially distributed and different parts of the fracture system are activated during different time intervals.

Fracture propagation timing

During the computation and integration of the depth volumes, a record is kept of the clock time at which each voxel is activated. This clock time of fracture activation is called Fracture Propagation (FP) and provides the time sequence of fracture opening. This allows for the tracking of the fracture formation over time through the volume and adds detailed knowledge of the fracture opening process that can be used in treatment design. Figure 10 shows the total stimulated fracture system near the frac stage location for the entire pumping time. The colors show the first time of activation for each part of the fracture. Notice that the first time of activation goes to the left early in the pumping and then progresses systematically to the right during the remaining time of pumping. The activation to the left happens in a very short time interval while the activation to the right side is incremental and spaced over the total pump time.

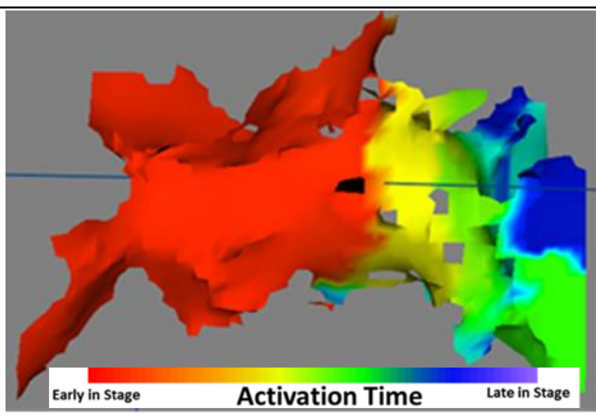

Figure 10: The induced fractures for the entire pumping time for the same frac stage shown in Figure 2. The colors show the first time of activation. The color scale shows the time from early in stage pumping to late in stage pumping. The earliest times are at the frac stage location along the well.

Predicting frac performance

Passive recordings during quiet times are used to image the seismic signals from the reservoir. These signals show the fractures that are active because of the production in the adjacent wells. One of the images that are computed from this quiet time passive data is the image of the larger area fractures. Mapping the locations where these fractures cross the new well predicts the stages of the treatment in the new well that will interact with the producing well. This is shown in Figure 11. The left panel in Figure 11 shows the volume of the reservoir that was activated during frac treatment of well A. The middle panel shows the fractures that are active caused by the production in well A with the overlay for the rock volume that was producing before the frac of well B. The right panel shows the rock volume that is producing around well A after the frac of well B. The fractures shown in the middle and right panels of Figure 11 predict which stages in the well B treatment will cause pressure hits in well A. The intersection of the fracture with the location of well B allow pressure transmission from well B to well A during the frac treatment. The locations predicted for the interaction with well A were actually recorded by the producing pressure and volume in well A during the frac of well B. The predicted stages of interaction were confirmed by the production performance for well A.

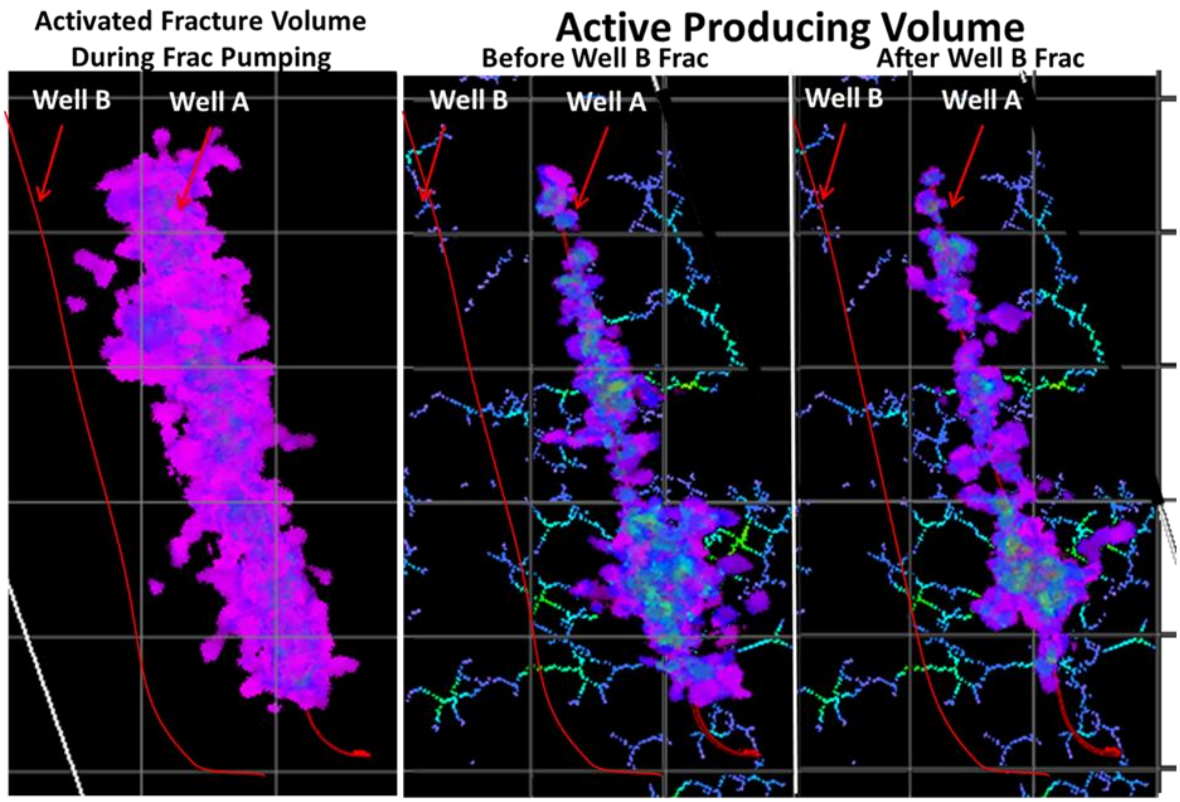

Figure 11: Predicting frac performance and computing producing volumes. The left image shows the total well activated volume with top down view for well A computed from passive data recorded while fracing of well A. Many months after well A started producing, the two images on the right are computed from quiet time passive data recorded before the frac treatment for well B. The computed fracture images show that the fractures cross well B is many locations and indicate the locations where the treatment of well B will interact with well A. The activated volume around well A during the quiet time is shown in the right hand image. This is the rock volume activated by the production from well A before the frac treatment of Well B.

Computing Active Producing Volume (APV)

The producing rock volume for well A was computed twice. The first volume was computed using quiet time recording before the frac of well B and again using quiet time recording after the frac of well B. The workflow for computing the producing volume tracks the activated voxels in the depth volume and passes only the active voxels that are connected to the well either directly or through other voxels. This is different from the fracture imaging workflow that maps the areal fractures. Figure 10 shows the two computed producing volumes overlaid on the areal fractures. The producing volume for well A after the frac of well B is 20% smaller than the producing volume computed before the frac of well B. The treatment of well B interacted with well A and caused the production from well A to drop.

Conclusions

We have presented a new approach for managing unconventional reservoirs. Using fracture imaging, the fracture systems in the reservoir are computed before the frac treatment, during frac treatment, and during production. Computing the producing volume at regular intervals over the years of production allows for better decisions on the design of the frac treatments for future wells and for the determination of where to do infill drilling. The installation of shallow buried grids over the reservoir provides for efficient recording of the data at the times required for monitoring frac treatments and for computing the producing volumes. A byproduct of the fracture imaging method is the ability to store the first time of activation for each segment of each fracture. This allows for detailed analysis of how the rocks are fracturing.

Computing the producing volume at regular intervals over time (4D) allows for better decisions in the design of the frac treatments for future wells and for the determination of where to do infill drilling. The installation of shallow buried grids over the reservoir provides for efficient data recording for the monitoring of frac treatments and for computation of producing volumes.

References

Das, I., and M. D. Zoback (2013), Long-period, long-duration seismic events during hydraulic stimulation of shale and tight-gas reservoirs -- Part 1: Waveform characteristics, Geophysics, 78(6), KS107-KS118.

Geiser P, Lacazette A, Vermilye J. Beyond ‘dots in a box’: an empirical view of reservoir permeability with tomographic fracture imaging. First Break 2012; 30 (July):63–69.

Lacazette A, Vermilye J, Fereja S, Sicking C. Ambient fracture imaging: a new passive seismic method. Unconventional Resources Technology Conference, Denver, CO, SPE 168849/URTeC 1582380; 2013. 10p.

Sicking C, Vermilye J, Geiser P, Lacazette A, Thompson L., Permeability field imaging from microseismic, SEG 1383; 2012. 5 p.

Sicking C, Vermilye J, Lacazette A, Yaner A, Klaus A, and Bjerke L., Case study comparing microearthquakes, fracture volumes, and seismic attributes. URTeC 1934623; 2014. 7 p.

Tary, J., and van der Baan, M., 2012, Potential use of resonance frequencies in microseismic interpretation, The Leading Edge, 31, 1338-1346.

Tary, J. B., van der Baan, M., and D. W. Eaton (2014), Interpretation of resonance frequencies recorded during hydraulic fracturing treatments, submitted to Journal of Geophysical Research.

.